Wake interactions in the large offshore wind development zone off the coast of Tamil Nadu, India

DTU Wind Energy
E-report

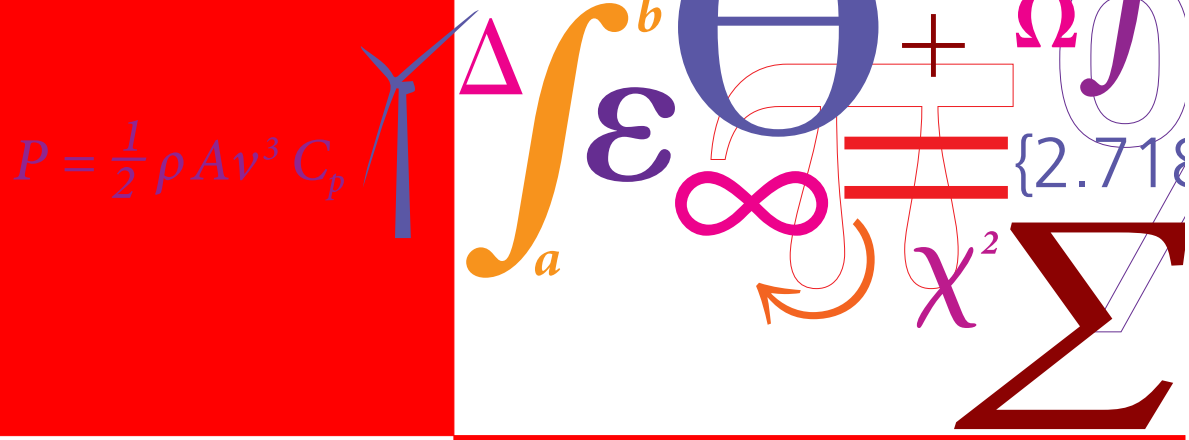

Jake Badger
Julian Antony Quick
Oscar M Garcia-Santiago
DTU Wind Energy E-0257
ISBN 978-87-87335-85-0
July 2025

DTU Wind Energy
Department of Wind Energy

Published by:
DTU, Department of Wind and Energy Systems, Frederiksborgvej 399, Building 118, 4000 Roskilde Denmark

www.wind.dtu.dk

Preface

This work is carried out by DTU Wind Energy, and commissioned by the Danish Energy Agency (DEA), in relation to DEA's collaboration with the National Institute of Wind Energy (NIWE). The purpose of this work is to investigate the impact of different considerations pertaining to the turbine layout of an offshore wind development zone off the coast of Tamil Nadu. For example, what impact does optimizing turbine layouts to give maximum annual energy production have? What impact does decreasing distances between wind farm "blocks" have on annual production. The scope is the geographical area of the planned development zone, and the prescribed wind farm "block" spatial definitions, and a single turbine type. The work uses two main wake modelling methods, the first provided by PyWake and the second by mesoscale meteorological modelling (similar to weather models). The modelling is provided for a single year (2020) chosen as the most representative year of a 30-year climatological period.

Contents

1 Executive Summary

The offshore wind development zone off the coast of Tamil Nadu presents an exciting opportunity to harvest the favourable wind conditions of this location. The favourable wind conditions are caused by mesoscale flow phenomena influenced by the terrain of the southern tip of India. Plans of deployment of wind energy at this scale requires careful consideration, because wind turbines convert some of the kinetic energy of the air flow into electrical energy (and other energy forms; heat, mechanical energy, etc.). The reduced kinetic energy is associated with the reduced wind speeds behind wind turbines and wind farms, and is known as the wake effect. It is necessary to study the influence of a large number of wind turbines on the flow, in order to quantify a realistic energy production of the development area. In doing this, a number of different approaches to mitigating electricity production losses due to wake effects can be investigated.

Four different wind turbine layout cases for the Tamil Nadu wind farm cluster have been tested for their performance characteristics using the WRF mesoscale model simulations, including the Explicit Windfarm Parameterization (EWP) developed at DTU Wind, for the representative year 2020. A reference simulation for 2020 with no wind turbine wake effects is also performed to provide wind climate statistics. Non-optimized and optimized turbine layouts are tested. The non-optimized layouts have a uniform 5 MW km^{-2} installed capacity density. The optimized turbine layouts preserve the same installed capacity per wind farm as the non-optimized. The optimized layouts optimize the total wind farm cluster Annual Energy Production using PyWake and Topfarm software. The individual wind farm performances are determined in terms of Annual Energy Production, wake losses, and Capacity Factor. Total wind farm cluster Annual Energy Production values are estimated and range from 79 TWh to 80 TWh; individual wind farm wake losses range from 14 % to 29 % and Capacity Factors range from 47 % to 58 %. Optimization of the layouts can increase the total production by about 1 %. Increasing the area of the wind farms by removing the edge exclusion zone increases total production by 0.3 % and 1 %, for optimized layouts and non-optimized layouts respectively. For the larger area wind farms (i.e. without the edge exclusion zone) optimization of the layouts can increase the total production by about 0.4 % . Overall, this study has been able to supply a detailed appraisal of wind farm cluster constituent farms' performances using the state-of-the-art modelling methodologies. It offers insights into consequences of decisions related to using buffer zone between wind farms, and using optimization of wind farm layouts. It also suggests relevant follow-up studies.

This study starts the process of understanding various trade-offs that will be part of planning this large offshore wind development zone. It is just the start though, because there are many other considerations, beyond wind resources, that need to be given attention in the planning process. These include, but are not limited to, seabed constraints, environmental considerations, structural loads, cabling constraints, costs related to installation, operation, maintenance, and decommissioning, levelized cost of energy considerations, market considerations (for example: the value of the electricity produced at the time it is produced) and the attractiveness to developers of each wind farm "block".

2 Introduction and background

In the lead up to this study, National Institute of Wind Energy (NIWE) had carried out a preliminary resource assessment analysis based on WAsP and identified 14 wind farm “blocks” close to the Tamil Nadu coast (Fig 1). In that original study the WAsP software (www.wasp.dk) was used in order to calculate the expected mean Annual Energy Production (AEP), including the impact of wind turbine wakes. In the WAsP software, wake losses are calculated with the PARK model [1, 2], a fast and relatively simple momentum deficit model. This approach works satisfactorily in giving estimates of wake losses for small wind farms. However, when wind farms become very large, new and more complex methods are needed to estimate how wind turbine wakes impact the wind flow and neighbouring wind farms, where the PARK model provides less accurate results than higher fidelity approaches [3]. The study commissioned by Agora Energiewende [4] was one of the earliest investigations to serve national planners, and energy stake-holders on these large-scale wind farm cluster wakes for wind energy deployment in the German Bight. Due to the size of the area, mesoscale modelling of wind farm wakes, was used in the study. This type of wake modelling has been compared to higher-fidelity approaches on simulating a proposed Energy Island’s wind farm cluster in the

North Sea obtaining similar results [5].

NIWE wishes to explore how Tamil Nadu's offshore resource can be exploited in a realistic and rational manner using, initially, a single target installed capacity, distributed in two different ways, and evaluated in terms of annual energy production using the very latest methods. This study uses state-of-the-art methods developed at DTU Wind and Energy Systems (DTU Wind), to investigate wake losses and layout optimization. The first uses the WRF (Weather Research and Forecast [6]) mesoscale model with the latest wind farm parameterizations from DTU Wind, called the Explicit Wake Parameterization (EWP, [7]). The second namely, TOPFARM [8] creates wind turbine layouts by optimizing the wind farm Annual Energy Production (AEP) and using PyWake [9] to account for wake effects. The use of these two different methods represents the state-of-the-art in wake modelling, and each has their strengths and weaknesses. By using and combining these approaches in this study, it is possible to determine a range of expected impact of the wakes on annual energy production.

This is appropriate for the purposes of the NIWE investigation, because, as will be explained in the next section, the method allows NIWE to begin to see whether choices made at aggregated wind farm cluster level can create better conditions for presenting attractive opportunities for individual wind farm developers, and at the same time, assure a good collectively rational use of the full development areas.

This study answers these questions:

- For a given mean installed capacity density (namely 5 MW km^{-2}) what is the estimated Annual Energy Production (AEP) for each of the 14 wind farm blocks, when accounting for wakes losses using the mesoscale modelling approach?
- What are the associated wind farm Capacity Factors?
- What is the level of lost production due to wake losses for each wind farm?
- Are there differences in these estimates if the wind farms are given a turbine layout with an even, nearly uniform, spacing between turbines, compared to turbine layouts that try to maximize the aggregated wind farm cluster Annual Energy Production (AEP)?

2.1 Offshore development zones

This study is based on predefined offshore development zones, shown with their numbering in Figure 1. The total area of the blocks is 3586 km^2, ranging in size from 203 km^2 for blocks 10 and 2, to 424 km^2 for block 13. The blocks have an approximate inter-farm distance of 1.3 to 1.5 km between the small blocks and from 2.0 to 3.3 km between the large blocks. Layouts are generated excluding or including a 500 m interior buffer zone. Here, 'excluding' refers that no turbine is located in this buffer zone and opposite for the term 'including'. Thus, the exclusion makes the total area smaller (3116 km^2 or 13 %) and increase the effective inter-farm distance. In this study, different ways of exploiting these development zones will be investigated.

Another prescribed input to this study is the total installed capacity of each wind farm block. This is defined in terms of a chosen installed capacity density and the area of each wind farm block. The chosen installed capacity density is 5 MW km^{-2}. Using the total area of the wind farms (before any exclusion of the 500 m interior buffer zone) results in a total installed capacity of 17.925 GW. The distribution of this total capacity is thus determined by the respective areas of each of the wind farm blocks.

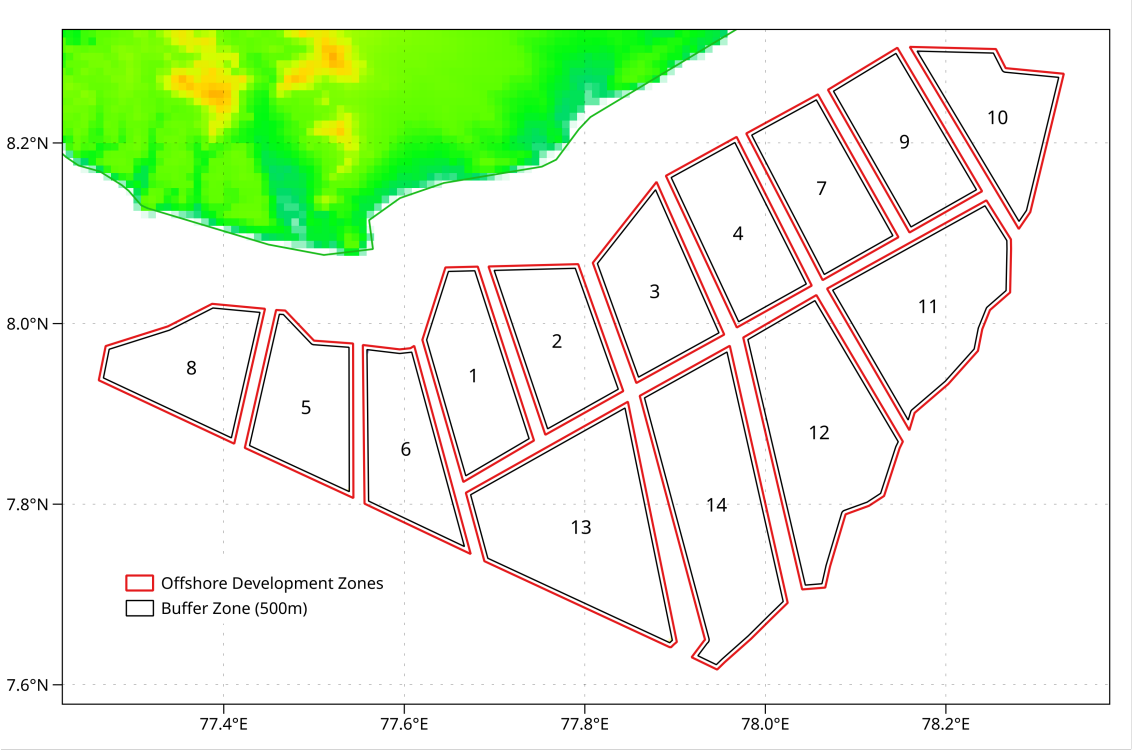

Figure 1: Proposed wind farm blocks for offshore wind farm projects off the Tamil Nadu coast.

3 Methods

In this section, details of the approach used to create wind farm turbine layouts and assess various properties of these layouts are given. Layout refers to the specific position, described by individual coordinates of each turbine for each wind farm block. The chosen technology used in this investigation is the IEA 15 MW reference turbine [10] with a hub height of 150 m and a rotor diameter of 240 m. This is a good choice because the necessary data is openly accessible, in particular, the power curve and thrust curve for which are shown in Figure 2. Using the capacity density stated means deploying 1195 turbines in total, distributed across the wind farm block in a number of different ways described below in Table 1 and shown schematically in Figure 3. In all cases, the model parameters, inputs, and post-processing procedures are kept constant, with only the turbine positions being different for each case.

3.1 Wind farm layout design

The study is broken down into three main cases. Case 0 is a simulation in which the flow is not impacted by wind farms at all. This can be seen as a reference case, providing the basic state conditions, before any wind farms are influencing the flow. Case 1 is a simulation in which the flow is impacted by wind farms using a uniform turbine layout. Case 2 is a simulation in which the flow is impacted by wind farms using the AEP optimized turbine layout. The layout is optimized for maximizing the full wind farm cluster annual energy production (of all 14 wind farm blocks).

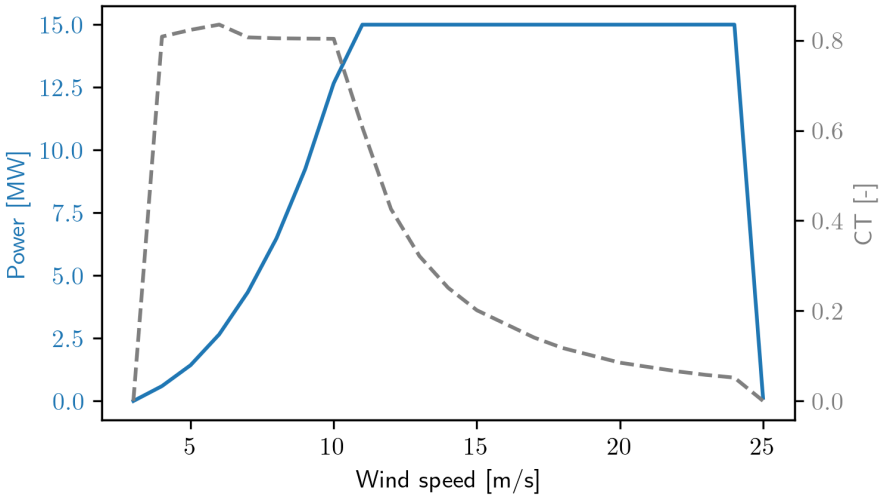

Figure 2: Thrust and power curves of the IEA 15 MW turbine.

Table 1: Table detailing the Case set-ups used in the study

Case	Number of Turbines	distribution	interior buffer
0	0 (reference run)	none	not relevant
1	1195	evenly	excluded
2	1195	to maximize total annual energy production	excluded
1z	1195	evenly	included
2z	1195	to maximize total annual energy production	included

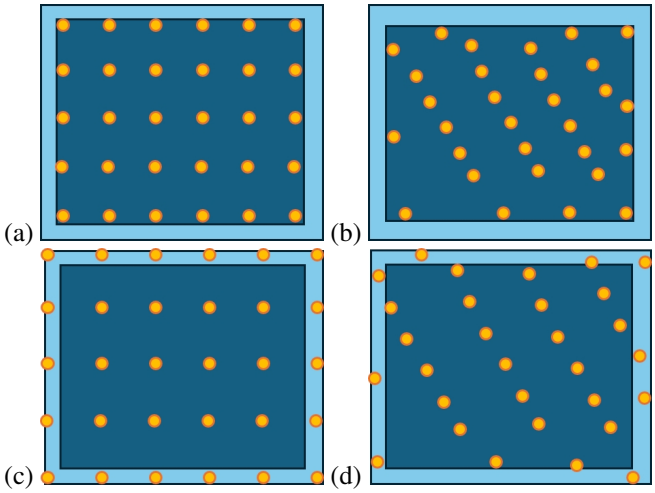

Figure 3: Figures schematically illustrating the different layout settings for the cases investigated in this study, illustrating (a) case 1 layouts, evenly distributed turbines excluding the interior buffer zone, (b) case 2 layouts, optimized distributed turbines excluding the interior buffer, (c) case 1z layouts, evenly distributed turbines including the interior buffer zone, (d) case 2z layouts, optimized distributed turbines including the interior buffer.

3.1.1 Layout based on homogeneous spatial density

Table 1 details the cases used in this study. For Case 1, the layouts are based on a cluster layout generating algorithm. With the polygons provided by NIWE (Fig. 1), the target capacity density (5 MW km^{-2}), and the chosen technology (IEA 15 MW), determines the total number of wind turbines per block. Then, the area is filled with random points, equal to the total number of wind turbines per block, and K-means clustering is applied to these points. The number of cluster is equal to that of wind turbines and the centroid of every cluster gives the new wind turbine positions. The process iterates until it converges (no change in positions), resulting in an evenly distributed layout with a uniform density.

The algorithm creates equally distanced turbine positions creating non-conventional layouts—the rows or columns are not straight lines perpendicular to the mean wind direction. Notice that this method optimizes for space and tries to locate the turbines as far as possible between them. The algorithm is advantageous as it reduces aliasing effects, and ad-hoc truncation of regular rows and column terminated by a irregular shaped wind farm "block" boundaries. The converged layout is reached without any consideration given to minimizing wake losses. More sophisticated optimizations, which consider wake effects and wind variability (time and space), are used for Case 2.

Figure 4 provides a visual representation of the converged layout using the mentioned algorithm. These layouts are used in the mesoscale simulations of Case 1. Table 2 lists some of the key specifications of each of these layouts, such as the number of turbines, minimum distance between turbines (expressed in rotor diameters, D), installed capacity, installed capacity density. Notice that for all wind farm blocks, the installed capacity density is kept as close to 5 MW km^{-2} as possible, which produces different installed capacity per block (Fig. 9). Except for blocks 11 to 14, all blocks have an approximate installed capacity of 1 GW. The largest block (no. 13) has an installed capacity of 2.12 GW in an area of 424.5 km^2. The entire cluster consists of a total of 1195 turbines with an average spacing of 5.9D and a total installed capacity of 17.96 GW.

Table 2: Case 1 wind farms and their respective areas, number of turbines, minimum distance between turbines (expresses in rotor diameters, D), installed capacity, installed capacity density. Note: for all the wind farms blocks the installed capacity density is kept as close to 5 MW km^{-2} as possible.

Block	Area [km^2]	No. turbines	Minimal distance [D]	Installed Capacity [GW]	Capacity Density [GW km^2]
1	208.3	69	5.8	1.04	4.97
2	202.9	68	5.8	1.02	5.03
3	208.9	70	6.1	1.05	5.03
4	208.1	69	6.0	1.04	4.97
5	206.6	69	6.1	1.04	5.01
6	203.7	68	5.7	1.02	5.01
7	208.1	69	5.7	1.04	4.97
8	206.9	69	6.2	1.04	5.00
9	204.1	68	6.3	1.02	5.00
10	202.8	68	5.8	1.02	5.03
11	329.5	110	5.9	1.65	5.01
12	380.1	127	5.9	1.91	5.01
13	424.5	141	5.5	2.12	4.98
14	391.4	130	5.8	1.95	4.98

Case 1 excludes the buffer zone; to investigate the inclusion of the buffer zone the same algorithm is used to produce the layouts for case 1z.

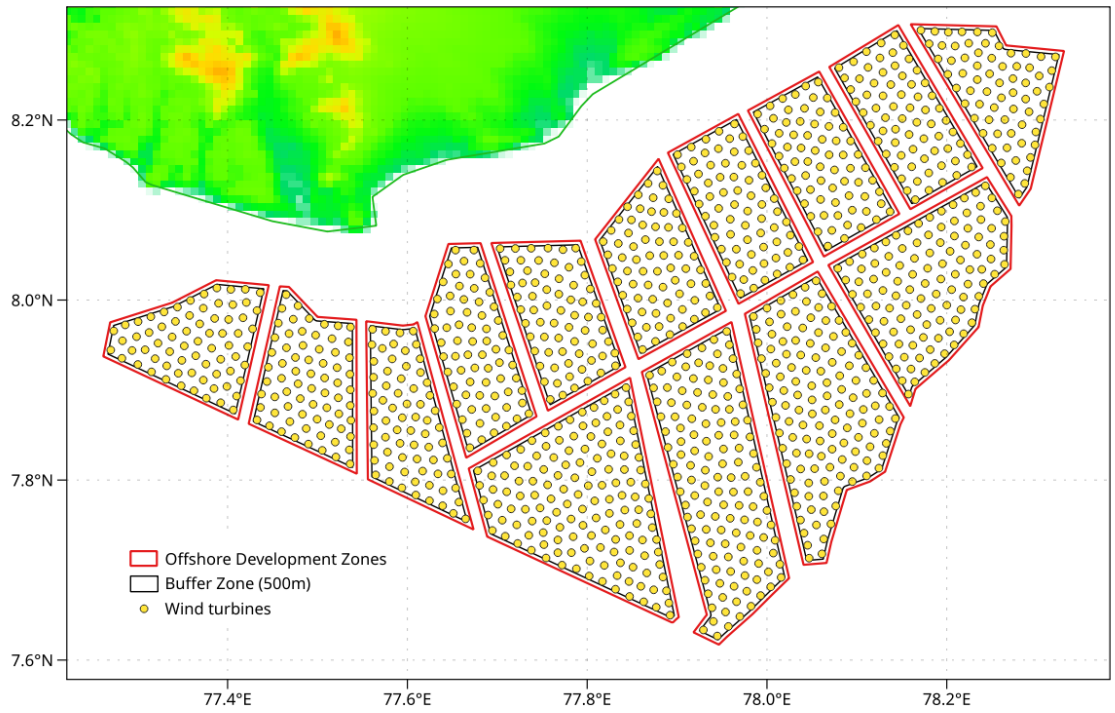

Figure 4: Wind farm layout for Case 1. The layouts ensure a capacity density of very close to 5 MW km^{-2} for each wind farm block. See main text for details of the method used to reach the layouts. Refer to Table 2 for details.

3.1.2 Layout optimisation using TOPFARM

Case 2 is using the optimized turbine layout maximizing the total wind farm cluster annual energy production. The optimization is performed using the TOPFARM stochastic gradient descent driver [11], using PyWake [9] to approximate wake effects. PyWake is run using the TurbOPark model [12, 13]. The TurbOPark model is an improved version of the PARK model which uses a Gaussian wake deficit and accounts for the wake expansion considering the ambient turbulence and the contribution from the wind turbines. The model has been validated in wind farms with neighbouring wind farm wake effects, showing good agreement with the SCADA data [12, 13]. When using the TurbOPark model within PyWake, wind speeds at the wind turbine locations (or local wind speed) is determined based on the results of the mesoscale simulations of Case 0. Then, wind turbine wakes are linear superimposed with the direction of each wake determined the local flow direction computed from Case 0. An example of the PyWake-modelled flow field is interpolated in Figure 7, showing a selected snapshot in time. Two optimized layouts where made using TOPFARM excluding and including the buffer zone (Figures 6 and 8 respectively)

In both Case 1 and Case 2 (and also Case 1z and Case 2z), the installed capacity density for each respective wind farm blocks is the same. The total installed capacity for each wind farm block is shown in 9. Looking at Fig. 8 it is possible to see the non-uniformity of the wind turbine spacing, with the appearance of alignment of turbine rows and alignment of elongated gaps between turbines, orientated perpendicular to the main flow directions.

3.2 Mesoscale modelling

Mesoscale modelling refers to scales of motions in the atmosphere from approximately 30 to 1 km in size. A mesoscale model can capture the dynamics of motions of the atmosphere and its thermodynamics, allowing

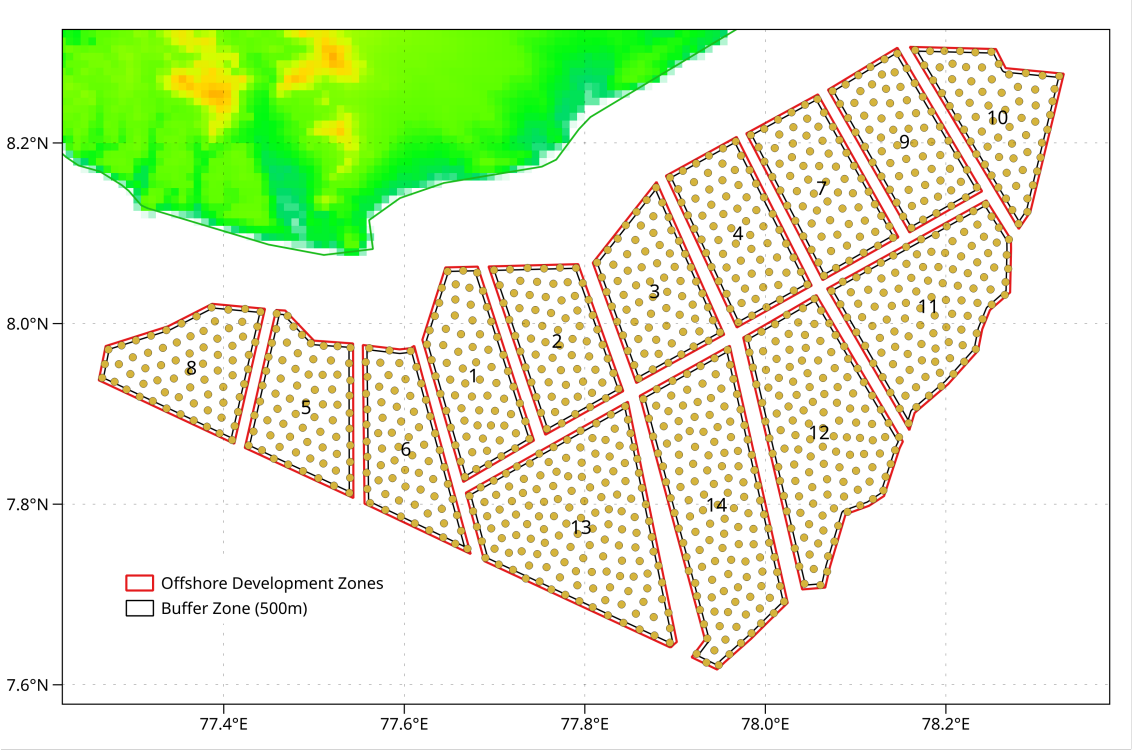

Figure 5: Wind farm layout for Case 1z.

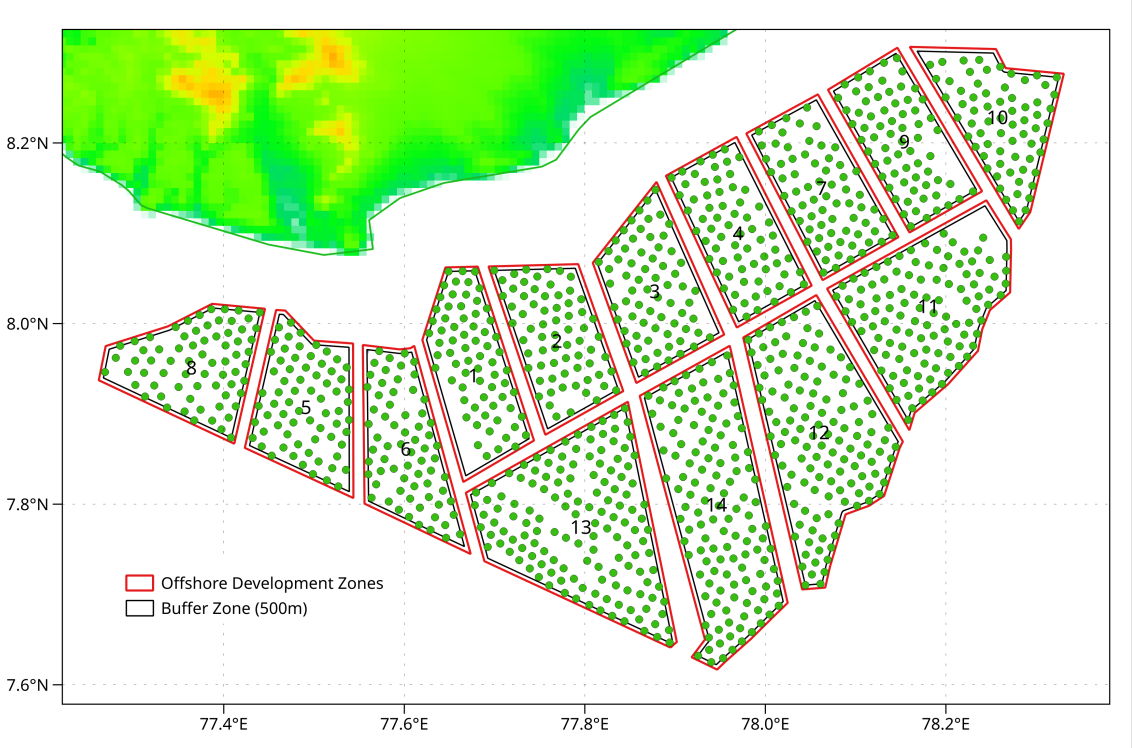

Figure 6: Wind farm layout for Case 2. Layout derived from TOPFARM.

it to simulate weather systems such as tropical cyclones. Most of the dynamics are solved by the model

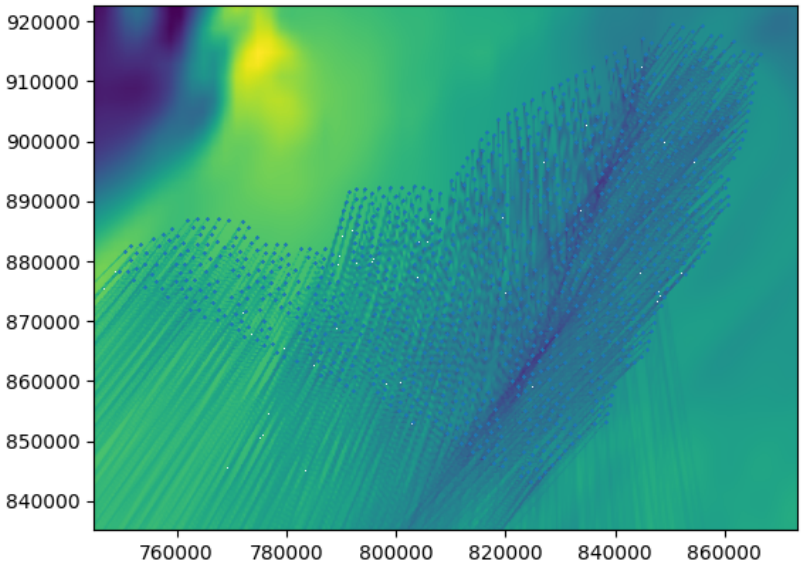

Figure 7: Wind farm flow modeled by PyWake using TOPFARM-derived layout for Case 2.

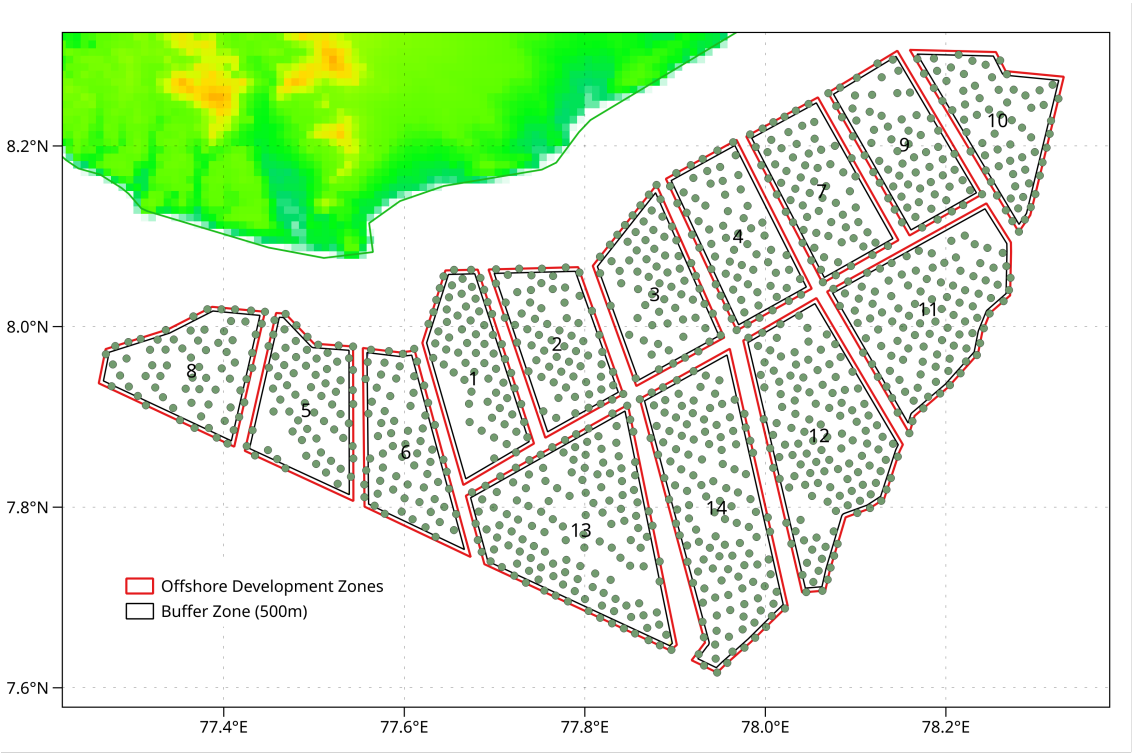

Figure 8: Wind farm layout for Case 2z. Layout derived from TOPFARM.

grid, whereas physical processes such as radiation, convection, or turbulence needs to be parametrised. The effects of wind farms in these models can be accounted for through parameterisations as the grid is not fine enough to solve the flow around the wind turbines.

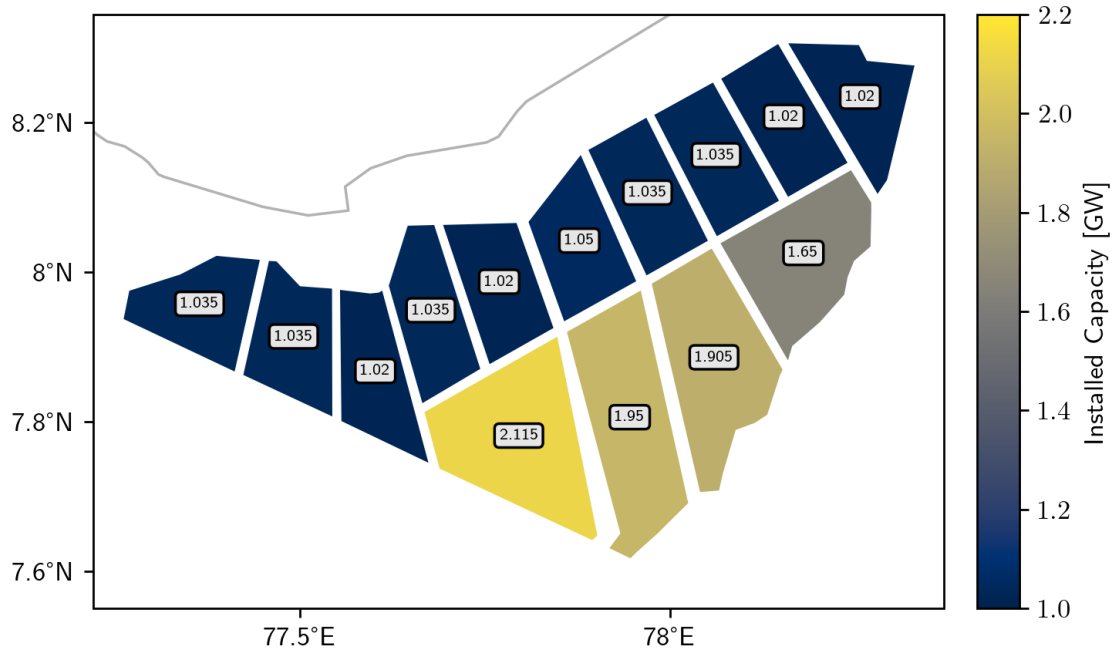

Figure 9: Installed capacity for each wind farm blocks, as given in Table 2 for details. This is the same for all cases, 1, 2, 1z and 2.

3.2.1 Mesoscale model setup

We use the Weather Research and Forecasting (WRF, [6]) mesoscale model version 4.2.2. Figure 10 shows the computational domains used with a focus on coverage of the southern part of the Tamil Nadu coast. The domain configuration consists of 3 one-way nested domains which means that the results from the outermost domain provides boundary conditions to the intermediary domain and then the intermediary domain to the innermost one. The domains have a resolution of 18, 6, and 2 km for the outermost, intermediary, and innermost domains, respectively (Domain 3, 2, and 1 in Fig. 10). The results are taken from the innermost domain (Fig. 11) with Fig. 12 showing the 2 km grid spacing over offshore development zones.

We choose a set of physical parameterizations similar to the NEWA's final configuration from [14] with modifications to the parameters of the Planetary Boundary Layer scheme. The forcing data for initial and boundary conditions come from ECMWF's ERA5 Reanalysis dataset [15] - ECMWF stands for European Center of Medium Range Weather Forecasting. The sea surface temperatures come from the Operational Sea Surface Temperature and Sea Ice Analysis (OSTIA, [16]). In each case, a full calendar year is simulated. It is split up into sets of 8 days where the last 24 hours of a set overlap with the first 24 hours of the following set. In each set, the first 24 hours will be discarded due to model spin-up. This methodology has been developed and extensively tested in projects in Europe ([**?**]) and South Africa ([17]) and elsewhere. In these referred to studies the estimates of wind speed distributions using this methodology were validated against high quality measurements (at present there are no published validation studies in any tropical waters for this methodology). The ERA5 data is used also used to provide nudging to the outermost domain (see 10).

3.2.2 Simulating wind farms in mesoscale models

The WRF mesoscale model cannot directly resolve the influence of wind turbines, due to the difference in scale between the model resolution and the scale of the turbines. Therefore, the influence of wind turbines needs to be parameterized in the mesoscale model. Two main parameterizations have been developed for this purpose in the WRF model. The Explicit Wake Parameterization (hereafter referred to as EWP, [7])

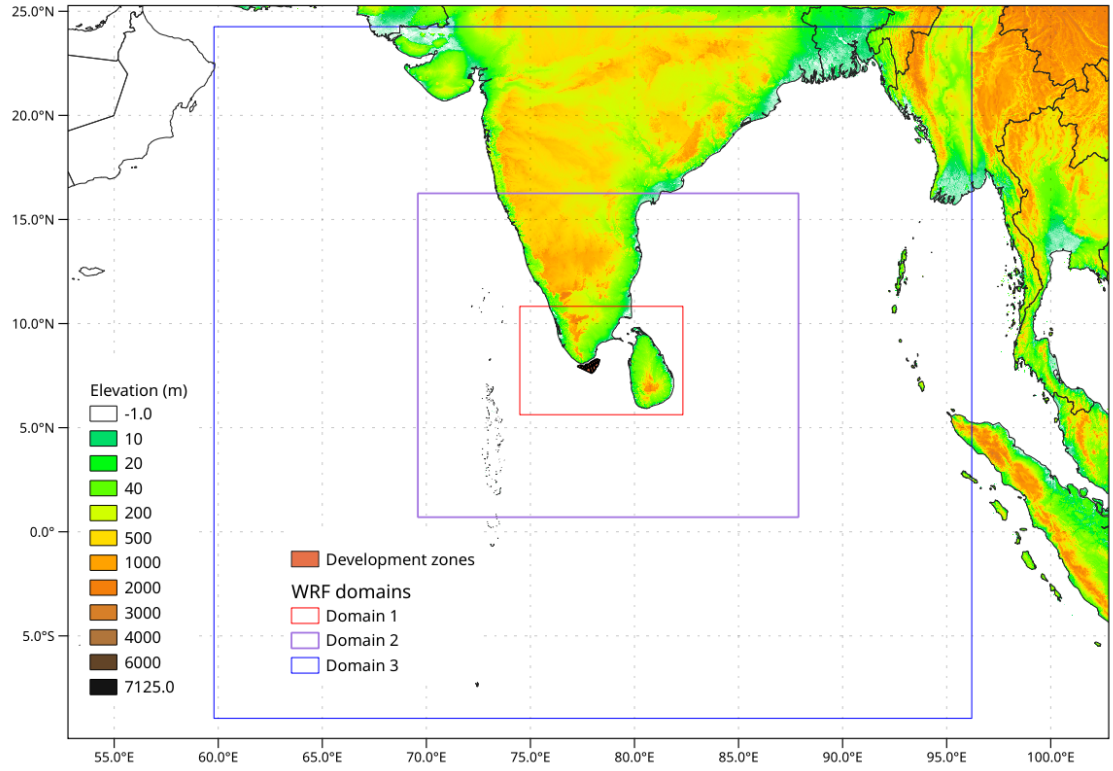

Figure 10: Map showing WRF's numerical modelling domains' configuration used for this study and the terrain elevation. The wind farm parametrization is applied in the innermost modelling domain (red frame).

and the Wind Farm Paramerization [18]. The EWP scheme is used with its default parameter for Case 1 and Case 2 as it has shown good agreement in wind farm cluster power loss when compared with high-resolution RANS simulations [5].

3.3 Selection of the representative year

It is common practice to use a year that represents the average conditions of the wind climate's region. It is also technically advantageous for the mesoscale modelling to simulate one year as it is not computationally feasible to run 30 years (standard climate period). To select the climatological year to run all cases, the ERA5 global dataset is used. The most recent 30-year climatology (1994–2023) is used and the selection process gives importance to 3 variables relevant for wind resource assessment and wakes: wind speed distribution, wind direction distribution, and atmospheric stability. The year-derived statistics for each variable is calculated and compared against the full 1994–2023 period for 8 randomly selected points in the southern part of Tamil Nadu (Fig. 13). Then, the year is ranked based on the objective measure given for each variable and all selected points. From this process, the year 2020 is selected, giving more weight to the wind speed variable and considering the closeness to present time. The random point approach is used because it enables the mesoscale meteorological flow phenomena to be appropriately sampled. If only the ERA5 gridpoints closest to the wind farms were chosen there is a risk that important variability on larger scales would be missed.

Figure 14 shows the comparison of the atmospheric stability and wind speed and direction distributions from the selected year 2020 obtained from point 7 in Fig. 13.

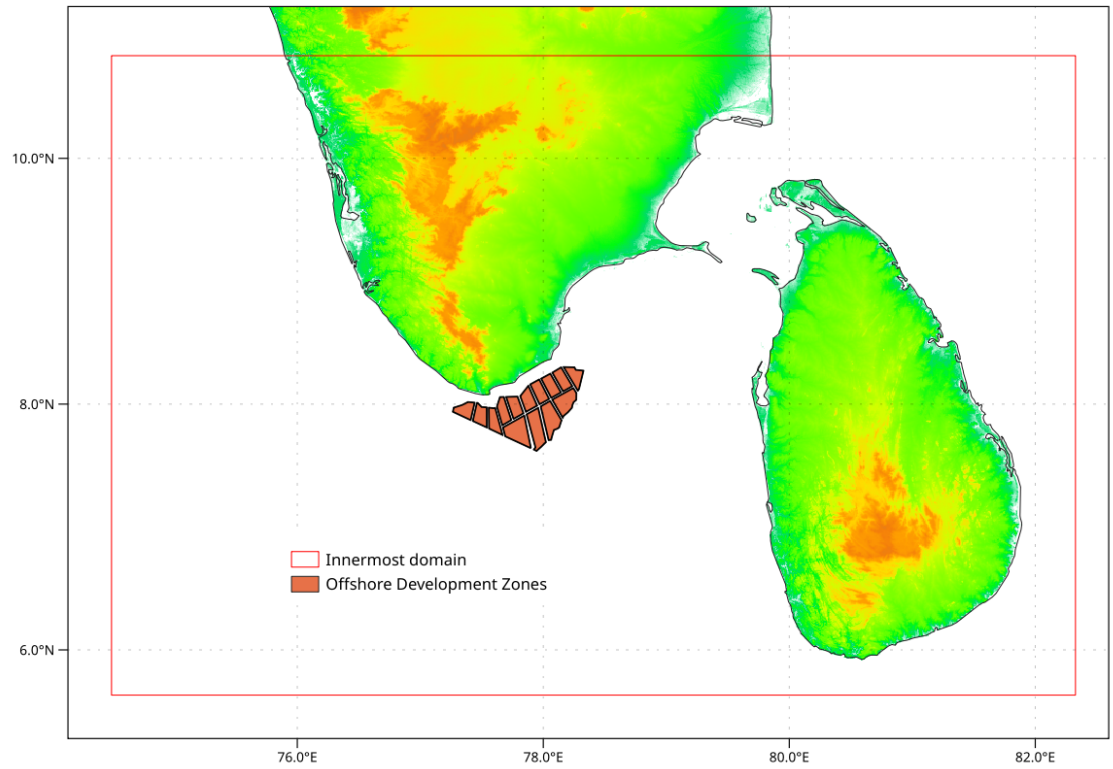

Figure 11: Map showing the extent of WRF's innermost modelling domain in more detail and the proposed offshore wind farm areas. Results are obtained from this modelling domain.

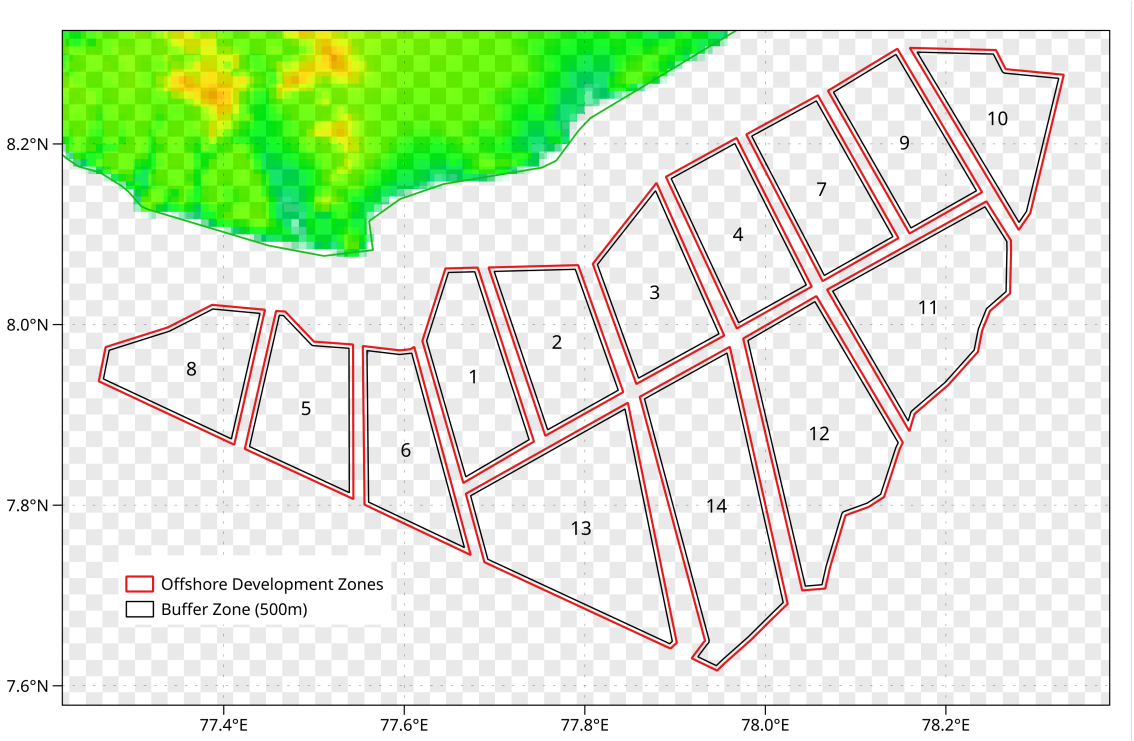

Figure 12: Example of the 2 km grid spacing from WRF's innermost domain with the proposed offshore wind farm areas.

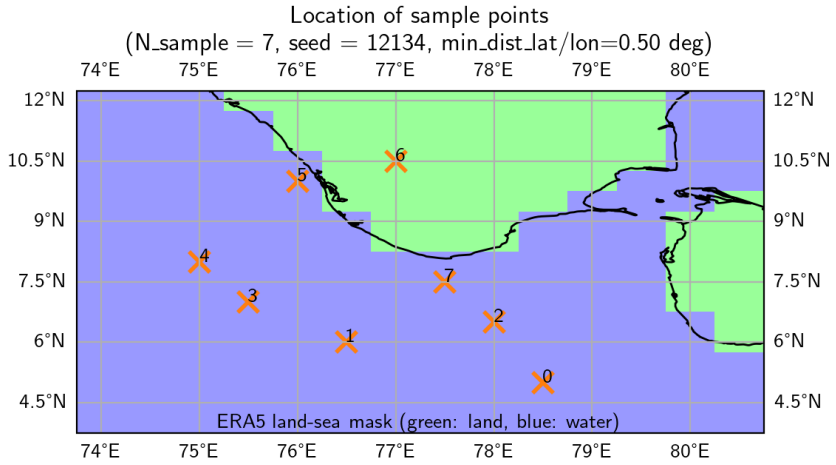

Figure 13: Map showing the random ERA5 reanalysis grip points used in the selection of the representative year. See main text for details.

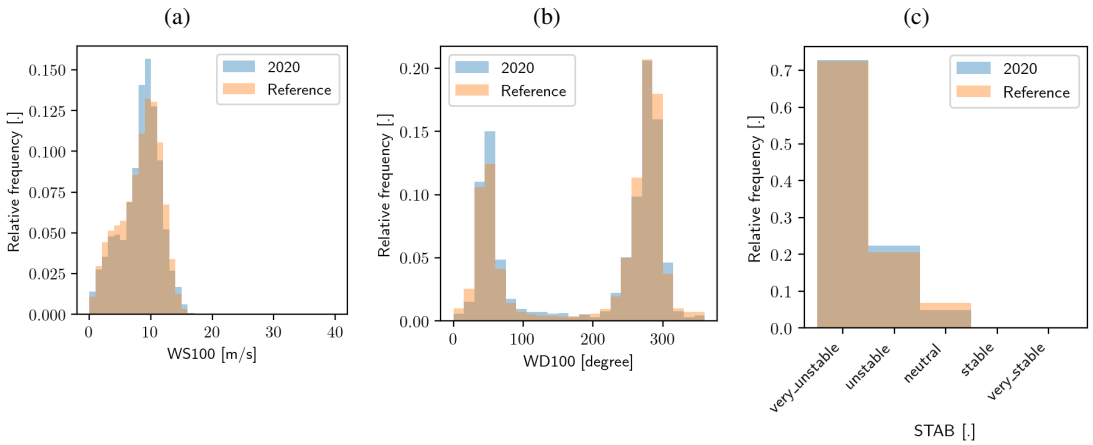

Figure 14: Comparison of distributions of wind speed (a), wind direction (b), and atmospheric stability (c) for the simulation year 2020 and the reference period. The data are obtained ECMWF ERA5 reanalysis (see main text for details) from the grid point located at the 7 points shown in Fig. 13.

4 Detailed results for each Case

4.1 Case 0: Mesoscale simulations without wind farms

Figure 15 shows the mean wind speed at 150 m. Blocks from 1,2 and 3 (and parts of blocks 6, 13, 14, 12 and 4) have wind speed area than 10 m s^{-1}. Most of the wind farm cluster has wind speeds exceeding 9 m s^{-1}. Only the extremities of block 8 and block 10 have wind speed below 9 m s^{-1}. Figure 16 shows the wind roses of each blocks extracted at the center of the area. All blocks show a bimodal distribution of the wind direction, with the west component (Northwest and Southwest included) the most frequent one, followed by the northeast direction. The predominant summer period wind direction comes from the westerly quadrant, with a variation slightly northwesterly at the western part of the wind farm cluster, to more southwesterly at the eastern part of the wind farm cluster. This indicates a turning of the wind through the wind farm cluster area during the summer period. In the winter period, the winds are predominantly from the northeast, and the turning wind across the wind farm cluster is not seen, as it was in the summer period. The strongest wind speeds are associated with the summer period, from the westerly quadrant.

Figure 17 shows the nominal Annual Energy Production (AEP) for each wind farm block derived from Case 0 simulations. As expected, the largest blocks (11–14) would nominally produce most power due to the higher installed capacity. Then, the approximately 1 GW blocks (1–10) have different production depending on the differing location specific wind climate. The variation in wind climate leads to blocks 1–3 produce more than 1 TWh more than block 10, the farm with lowest nominal Annual Energy Production (AEP).

Nominal Capacity Factors (CF) range from 56 % to 70 % in the whole wind farm cluster with blocks 1 and 2 showing the highest and block 10 the lowest. Please remember that these estimates do not account for wake losses, so these values are not an estimate of realizable production, but instead serve as a reference value to compare against. Also remember that the lower nominal production of block 10 is due solely to the wind climate variation across the wind farm cluster area, i.e. even before accounting for wake effects.

CASE 0

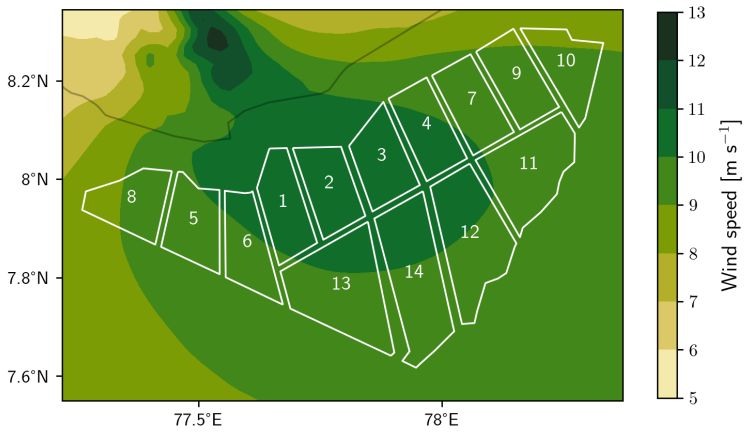

Figure 15: The average wind speed for the year 2020 at 150 m above surface level from the mesoscale simulation for Case 0.

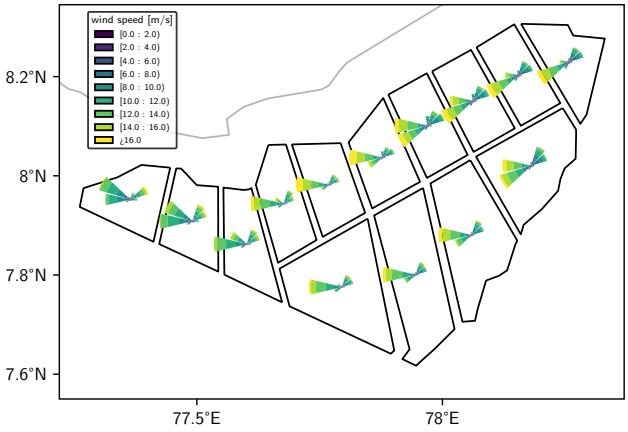

Figure 16: Wind speed and direction at 150 m above surface level presented as wind rose per each wind farm block. Wind roses are created from the times-series extracted from the centroid of each wind farm block.

CASE 0

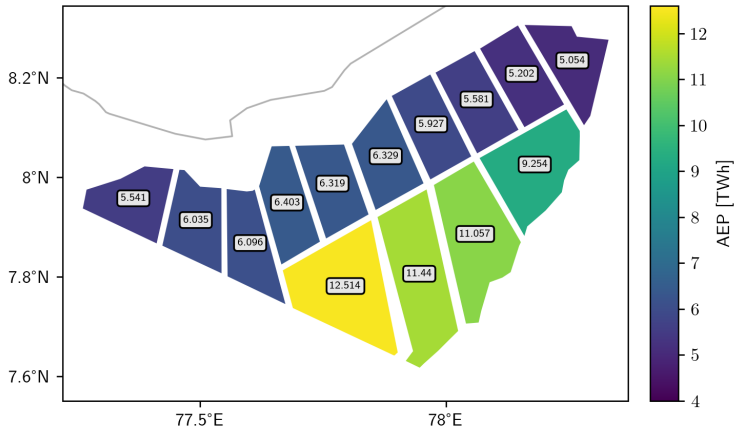

Figure 17: Gross or nominal Annual Energy Production (AEP) for each wind farm block from Case 0 simulations. IMPORTANT: this notional value takes NO ACCOUNT of wake effects. The nomimal power uses the wind speeds at the turbine locations and uses the turbine power curve, but no thrust (deceleration) is imposed on the flow.

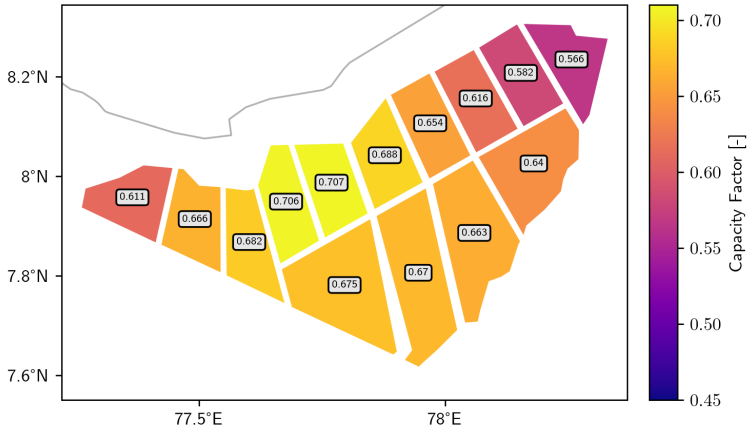

Figure 18: Nominal capacity factor for each wind farm block from Case 0 simulations. IMPORTANT: this notional value takes NO ACCOUNT of wake effects. The nomimal power uses the wind speeds at the turbine locations and uses the turbine power curve, but no thrust (deceleration) is imposed on the flow.

4.2 Case 1: Mesoscale simulations with non-optimized wind farms and interior buffer excluded

The total effect of the wind farms is reflected in the mean wind speed at 150 m, shown in Figure 19, for the same climatological year as in Case 0.

Figure 20 shows the difference in wind speed caused by the wind farms and the extension beyond the the development zone. The largest reduction in mean annual wind speed differences (2 m s^{-1} reduction) are in blocks 12 and 14. Since the most frequent wind direction comes from the west, the largest block (no. 13) is only partially under non-wake-affected winds. However, it produces wakes that affect largely blocks 12 and 14. The wind speed difference is a result of the non-linear relationship between wind speed and turbine thrust, and terrain effects at the mesoscale creating flow accelerations over the wind farm cluster. Outside of the wind farm cluster, particularly in the northeast and southwest direction there is an extended region with wind speed reduction (>0.4 m s^{-1} reduction).

The Annual Energy Production (AEP) including wake effects is shown in Fig. 21. Due to wake effects, the production falls from 12.5 to 9.2 TWh in the largest block (no. 13) and its reduced ≈1.4 TWh for block 1 and 2. It is easier to appreciated the wake losses in Fig. 22. The wake losses range from 15 % in block 8 (westernmost wind farm block) to 29 % in block 12 (to the northeast of blocks 13 and 14).

As indicated in Figure 20, the mean wind speed does not continue reducing when moving through wind farm blocks 1 to 7, i.e. spanning the central northern region of the wind farm cluster. This may be partly due to the bidirection wind direction climatology, and the meteorological phenomena enhancing the flow in the region, related to the presence of high terrain on the Indian southern tip. This leads to a fairly uniform wake loss value of around 20 % for wind farm blocks 1,2,3,4 and 7.

An example of an interesting feature is the comparatively high wake loss for wind farm block 6 (24.5 %) compared to wind farm block 7 (19.3 %). Both wind farms could be described as the third from either west or east end of the wind farm cluster, and have comparable AEP (4.602 TWh and 4.501 TWh respectively). Although wind farm block 6 is has someone greater wakes losses compared to wind farm block 7, it still has a slighly larger annual energy production compared to wind farm block 7.

The results' description for this case is completed here with Capacity Factors, show in Fig. 23. The greatest CF is for wind farm block 2 (with 56.2 %), the lowest CF is for wind farm block 10 (with 46.8 %). Also note that the CF for wind farm block 12 (with 46.9 %) is only slight higher than that for wind farm block 10. It is likely that wind farm block 10 is mainly affected by the lower wind speed climate of its location in the first place, while wind farm block 12 is affected by having close neighbour wind farms from the main directions it receives wind from.

All these results show the complexity of the different responses to the interaction within the wind farm cluster. Farms with relatively low wake losses are seen together with the lowest CF of the wind farm cluster (block 10). This underlines the need to look at all of these results in order to understand the performance behaviour of each wind farm block.

CASE 1

Figure 19: The average wind speed for the year 2020 at 150 m above surface level from the mesoscale simulation for Case 1.

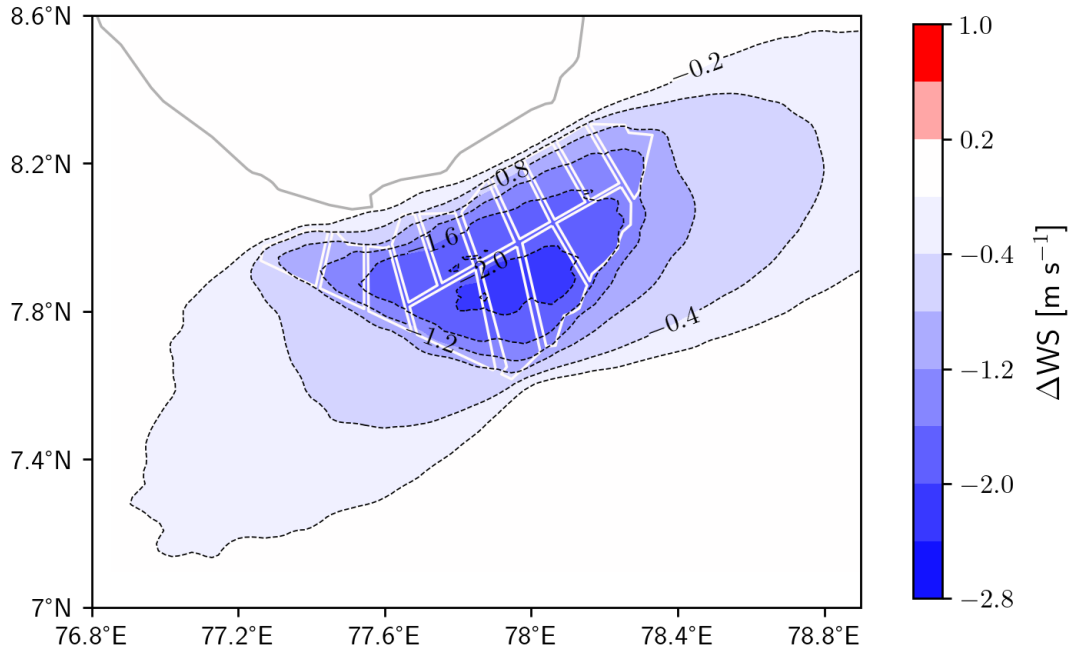

Figure 20: Mean wind speed difference at 150 m above surface level between Case 1 minus Case 0. This map shows the wake wind speed deficit over and around the wind farm cluster area.

CASE 1

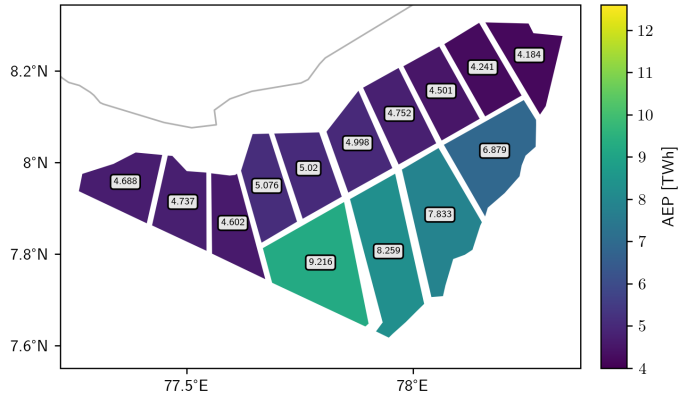

Figure 21: Net Annual Energy Production (AEP) for each wind farm block from Case 1 simulations. This estimate accounts for wake effects.

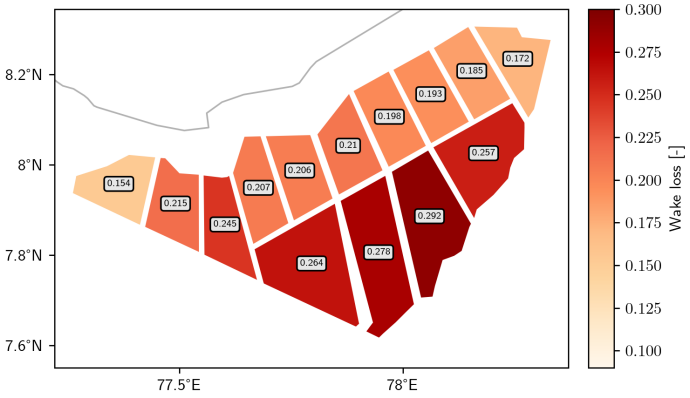

Figure 22: Wake loss, expressed as decimal fraction, for each wind farm block from Case 1 simulations. Note, a value of 0.2 is equal to 20 % wake losses.

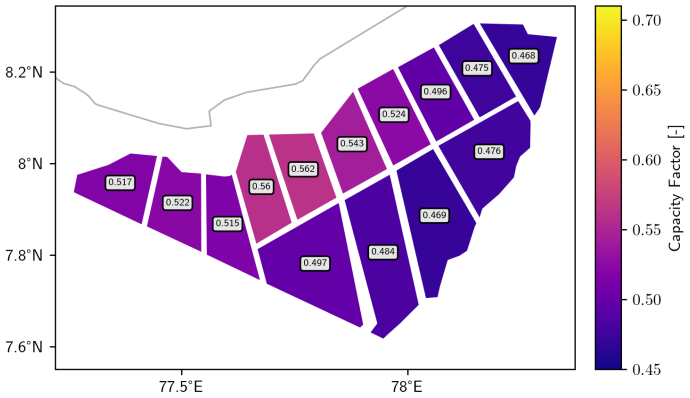

Figure 23: Capacity factor for each wind farm block from Case 1 simulations. Compare with Figure 18 for the values for Case 0.

4.3 Case 2: Mesoscale simulations with optimized wind farms and interior buffer excluded

In Figure 24 the total effect of the wind farms is reflected in the mean wind speed at 150 m. There is a noticeable difference in the 7 m s^{-1} contour in wind farm blocks 13, 14, 12 and 10, compared to Case 1 (Figure 19). This indicates the wake deficit is slightly lower in these wind farm blocks. The difference may be quite small however, because the contour placement can change quite dramatically where wind speed gradients are small.

Figure 25 shows the largest wind speed differences (2 m s^{-1} reduction) are in blocks 12 and 14, the area with 2 m s^{-1} reduction or greater appears smaller and more fragmented in comparison to Case 1 (Figure 20) Similar to what was seen in Case 1, outside of the wind farm cluster, particularly in the northeast and southwest direction there is an extended region with wind speed reduction (>0.4 m s^{-1} reduction).

The Annual Energy Production (AEP) including wake effects is shown in Fig. 26. For Case 2 in the largest wind farm block, block 13, the production falls from nominal 12.5 TWh to 9.409 TWh, compared to 9.216 TWh in Case 1. The production is reduced ≈1.3 TWh for block 1 and 2. This is slightly smaller difference compared to Case 1.

In Fig. 27, it is seen that the wake losses range from 15 % in block 8 (westernmost wind farm block) to 28 % in block 12 (to the northeast of blocks 13 and 14). This is a just a little less than in Case 1.

As was seen before in Case 1, there is fairly uniform wake loss value of around 20 % for wind farm blocks 1,2,3,4 and 7.

As in Case 1, there is a comparatively high wake loss for wind farm block 6 (23.9 %) compared to wind farm block 7 (19.4 %). Both wind farms could be described as the third from either west or east end of the wind farm cluster, and have comparable AEP (4.641 TWh and 4.499 TWh respectively).

The results' description for this case is completed here with Capacity Factors, show in Fig. 28. The greatest CF is for wind farm block 1 (with 57.6 %). For Case 1 it was wind farm block 2 (with 56.2 %). The lowest CF is still for wind farm block 10 (with 47.3 %) (compared to 46.8 % in Case 1). Also note that the CF for wind farm block 12 (with 47.4 %) is only slight higher than that for wind farm block 10, as it was also for Case 1.

CASE 2

Figure 24: The average wind speed for the year 2020 at 150 m above surface level from the mesoscale simulation for Case 2.

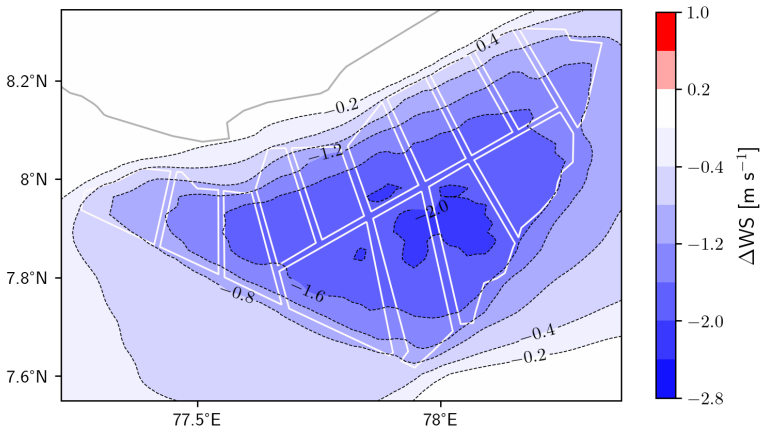

Figure 25: Mean wind speed difference at 150 m above surface level between Case 2 minus Case 0. This map shows the wake wind speed deficit over the wind farm cluster area.

CASE 2

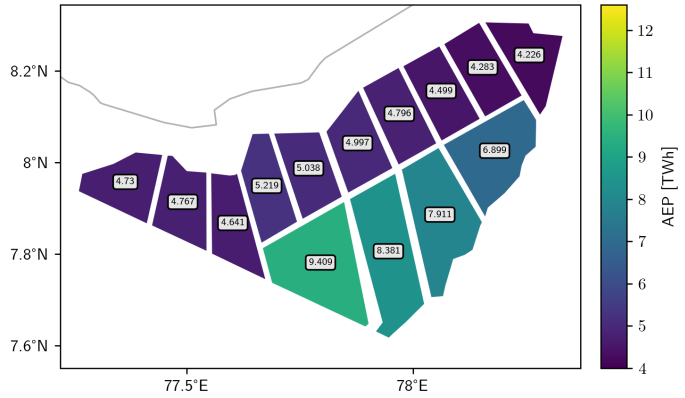

Figure 26: Net Annual Energy Production (AEP) for each wind farm block from Case 2 simulations. This estimate accounts for wake effects.

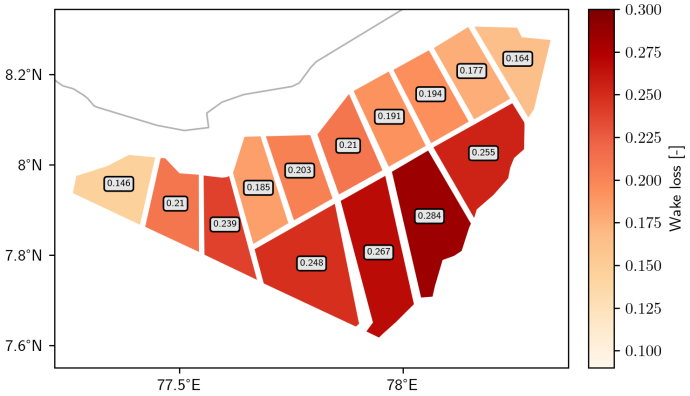

Figure 27: Wake loss, expressed as decimal fraction, for each wind farm block from Case 2 simulations. Note, a value of 0.2 is equal to 20 % wake losses.

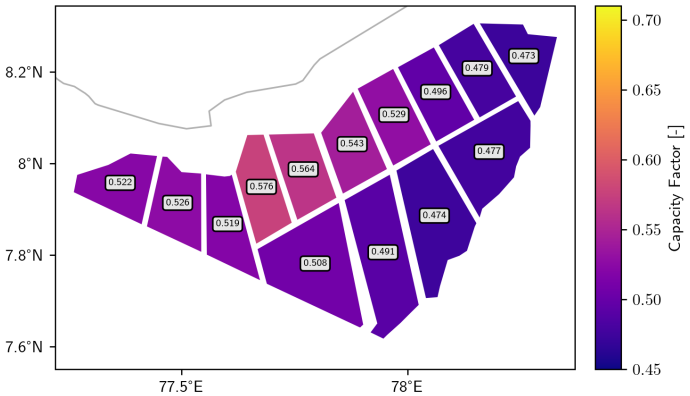

Figure 28: Capacity factor for each wind farm block from Case 2 simulations. Compare with Figure 18 for the values in Case 0.

4.4 Case 1z: Mesoscale simulations with non-optimized wind farms and interior buffer included

Case 1z offers an alternative evaluation of the annual energy production when not excluding the internal 500 m buffer zones. The resulting wind speed, wind speed deficits, AEP, wake loss, and capacity factor are shown in Figures 29 to 33.

In Figure 29 the total effect of the wind farms is reflected in the mean wind speed at 150 m. There is a noticeable difference in the 7 m s^{-1} contour in wind farm blocks 13, 14, 12, 11, and 10, compared to Case 1 (see Figure 19. This indicates the wake deficit is slighly lower in these wind farm blocks. The difference may be quite small however, because the contour placement can change quite dramatically where wind speed gradients are small.

Figure 25 shows the largest wind speed differences (2 m s^{-1} reduction) are in blocks 12 and 14, and some in block 12. the area with 2 m s^{-1} reduction has, in general, a similar form, but is slightly smaller, in comparison to Case 1 (Figure 20) Similar to what was seen in Case 1, outside of the wind farm cluster, particularly in the northeast and southwest direction there is an extended region with wind speed reduction (>0.4 m s^{-1} reduction).

The wind farm blocks' Annual Energy Production (AEP) for Case 1z, shown in Fig. 31, are all slightly higher than in Case 1, because of the larger area exploited and therefore slightly larger spacing between turbines. It follows that Wake losses are correspondingly lower, and capacity factor correspondingly higher too, shown in Figures 32 and 33.

CASE 1z

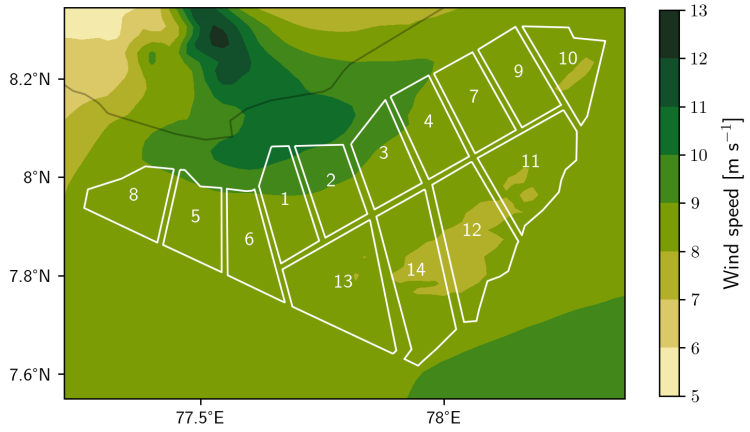

Figure 29: The average wind speed for the year 2020 at 150 m above surface level from the mesoscale simulation for Case 1z.

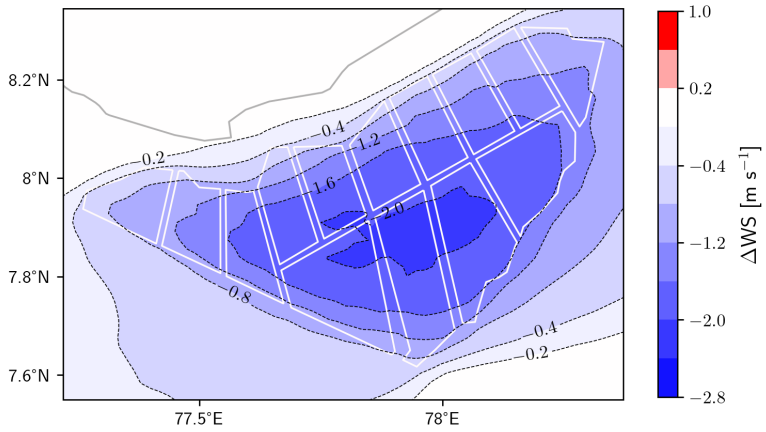

Figure 30: Mean wind speed difference at 150 m above surface level between Case 1z minus Case 0. This map shows the wake wind speed deficit over the wind farm cluster area.

CASE 1z

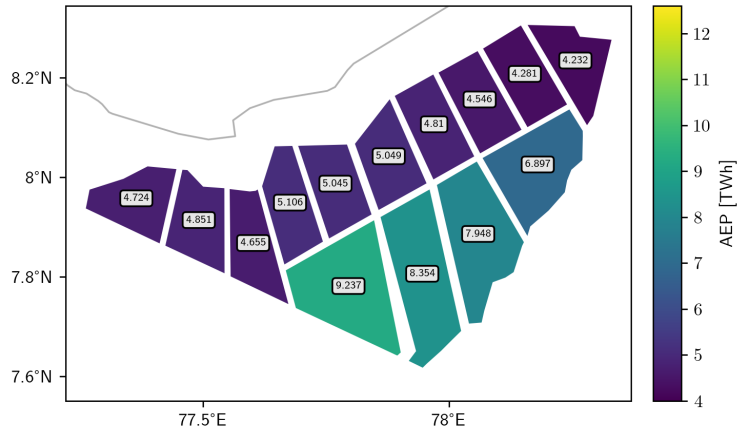

Figure 31: Net Annual Energy Production (AEP) for each wind farm block from Case 1z simulations. This estimate accounts for wake effects.

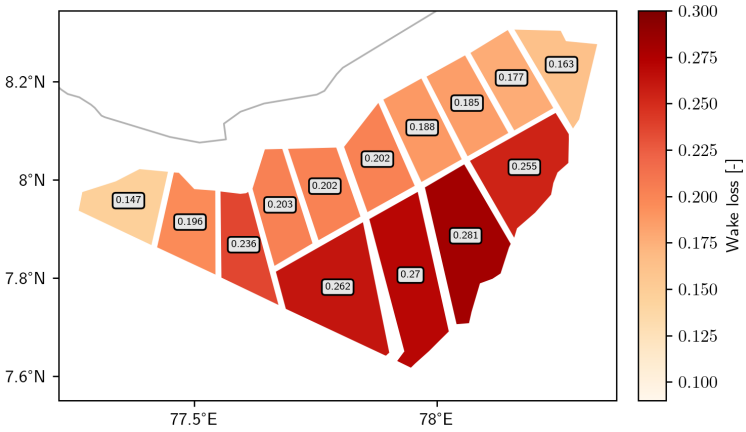

Figure 32: Wake loss, expressed as decimal fraction, for each wind farm block from Case 1z simulations. Note, a value of 0.2 is equal to 20 % wake losses.

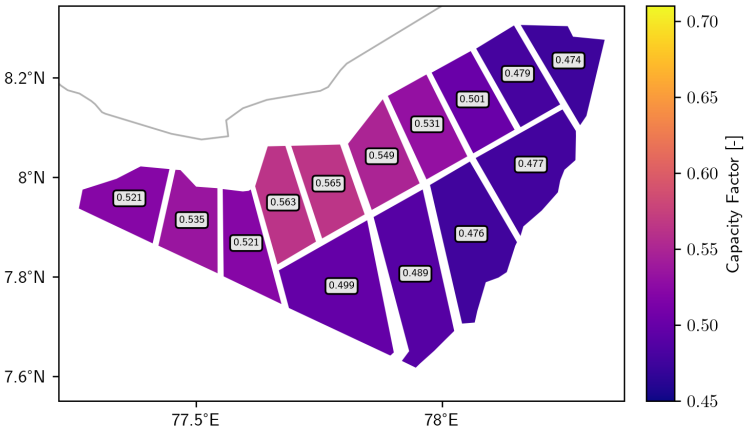

Figure 33: Capacity factor for each wind farm block from Case 1z simulations. Compare with Figure 18 for the values in Case 0.

4.5 Case 2z: Mesoscale simulations with optimized wind farms and interior buffer included

Here the results for the wind farm performance using the layout shown in Figure 8 are presented. The resulting wind speed, wind speed deficits, AEP, wake loss, and capacity factor are shown in Figures 34 to 38.

In Figure 34 the total effect of the wind farms is reflected in the mean wind speed at 150 m. There is a small difference in the 7 m s^{-1} contour in wind farm blocks 14, 12 and 11, compared to Case 1z (see Figure 29. This indicates the wake deficit is very slighly lower in these wind farm blocks.

Figure 35 shows the largest wind speed differences (2 m s^{-1} reduction) are in blocks 12 and 14, the area with 2 m s^{-1} reduction or greater appears slighly smaller in comparison to Case 1z (Figure 30) Similar to what was seen in all the other cases, outside of the wind farm cluster, particularly in the northeast and southwest direction there is an extended region with wind speed reduction (>0.4 m s^{-1} reduction).

As was seen in the results of Case 2 compared against Case 1, for Case 2z compared against Case 1z, that overall the optimized layout shows a very slight increased annual energy production compared to the Case 1z results, Figure 37. However, some wind farm blocks actually gave a reduced AEP (wind farm blocks 2, 3, 4, 7, 11, 12). This change is also reflected in the same wind farm blocks have higher wakes losses (or the same at the number precision level) and lower capacity factors (or the same at number precision level), compared to Case 1z.

In the next section more aggregated analysis of the results across the cases will be summarized.

CASE 2z

Figure 34: The average wind speed for the year 2020 at 150 m above surface level from the mesoscale simulation for Case 2.

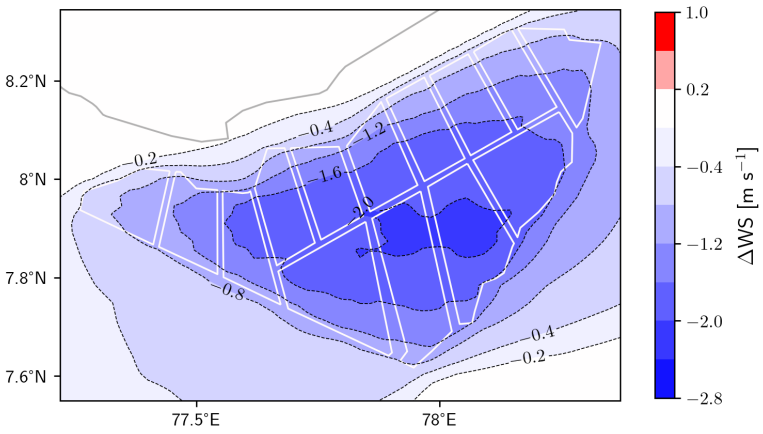

Figure 35: Mean wind speed difference at 150 m above surface level between Case 2 minus Case 0. This map shows the wake wind speed deficit over the wind farm cluster area.

CASE 2z

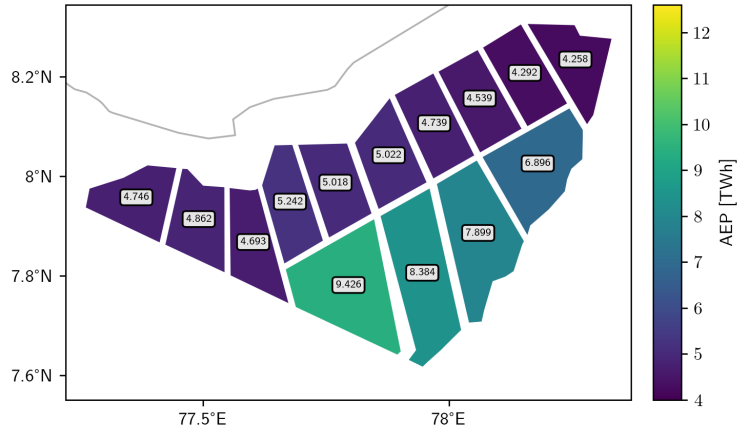

Figure 36: Net Annual Energy Production (AEP) for each wind farm block from Case 2 simulations. This estimate accounts for wake effects.

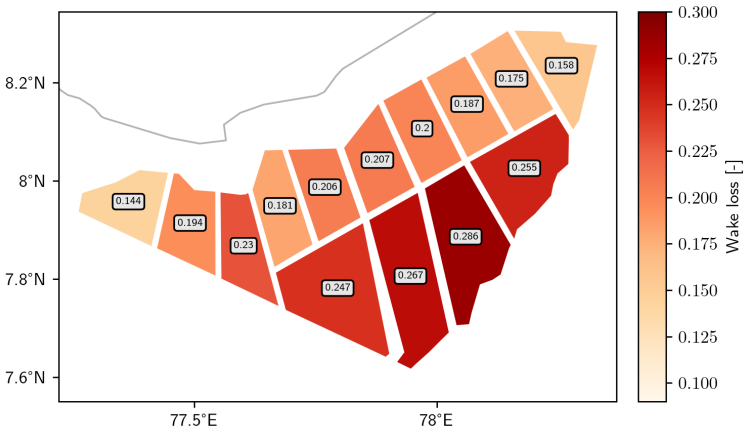

Figure 37: Wake loss, expressed as decimal fraction, for each wind farm block from Case 2 simulations. Note, a value of 0.2 is equal to 20 % wake losses.

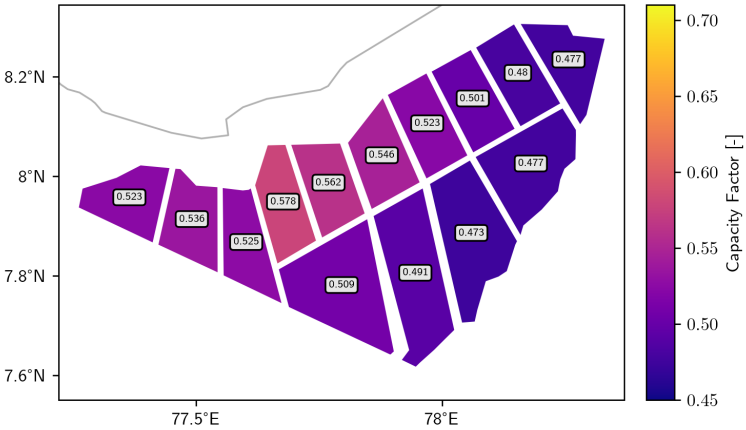

Figure 38: Capacity factor for each wind farm block from Case 2 simulations. Compare with Figure 18 for the values in Case 0.

5 Results in aggregate

For completeness, many plots have been presented and described to the reader. This was done so that it is possible to delve into the individual results and understand better the particular behaviour of one wind farm block against another, with the awareness of its relative position in the wind farm cluster, and the variation of the flow in terms of wind speed and direction.

In this section a more aggregated analysis of the results is given. In Tables 3, 4 and 5 is given the net annual energy production, wake losses, and capacity factors respectively. The tables give the results per wind farm block and for the entire wind farm cluster.

First, examining Table 3 it is seen that changing the layout from non-optimized to optimized, in the mesoscale modelling simulations, increases in the Annual Energy Production by 1.0 %, (i.e. going Case 1 and Case 2).

Next, the effect of increasing the wind farm blocks can be evaluated for the non-optimized and optimized wind farm cluster. For the non-optimized wind farm clusters, increasing areas used gave a 0.95 % increase in production. For the optimized wind farm clusters, increasing the area used gave 0.28 % increase in production.

Comparing the Annual Energy Production using the larger area and going from non-optimized wind farm cluster to optimized wind farm cluster gives a 0.35 % increase in production, (i.e. going from Case 1z to Case 2z).

For the Case 2z case it is seen that wind farm blocks 2, 3, 4, 7, 11, and 12, exhibit a reduction in production compared to the Case 1z. Saying that the optimization of the layout for the wind farm cluster, actually reduces the production of a selection of wind farms. Although this may seem initially counter-intuitive, it can be reasoned that a reduced performance of one wind farm block can lead to an increased performance of another wind farm block. The overall performance increases if the farms with increased performance outweigh the farms with decreased performance.

Comparing the wake losses across the wind farm blocks and cases, gives consistent description of what is described above. Compared to the nominal Annual Energy Production (i.e. no wind farm wakes accounted for) the non-optimized layout has wake loss of 23 % as is shown in the bottom line of Table 4. For the optimized layout the wake losses reduce to 22 %. Increasing the wind farm areas decreases the wake losses for both the non-optimized and the optimized layouts. However, the effect of increasing size is more marked for the non-optimzed layouts. Consistent with the AEP description, for some wind farm blocks the wake losses actually increase for the optimized wind farm cluster layout of Case 2z, compared to Case 1z.

To compare Capacity Factors across the wind farm blocks and cases, Table 5 is given. Here, a change in the best and worst performance, in terms of capacity factor, when going from non-optimized layout to optimized layout, can be seen. For Case 1 and Case 2, taking wind farm block 1, the optimization results in a bigger reduction in wakes losses, compared to the reduction in wake losses for wind farm block 2. Thus the leading performance moves from wind farm block 2 to wind farm block 1.

In the larger wind farm area cases (Case 1z and Case 2z), the change is even further marked, because the optimized wind farm cluster layout actually leads to a larger wake loss for wind farm block 2.

Finally, the total Annual Energy Production values given by PyWake for the different case is compared. These values are given in Table 6. The values from PyWake are consistently higher, by about 10 %. Because the two different methods use very different conceptual approaches to calculate the wake losses, we would not necessarily expect the same estimate from the two methods. PyWake is modelling the wind speed deficits from each wind turbine, assuming some generic properties of how the wind speed deficit changes with distance from its original wind turbine. Also this wake and its deficit propagates in a fixed wind direction from its origin, impacting downwind turbines in a straight line. Whereas, the mesoscale modelling models wind speeds modified by an aggregated wind turbine thrust at the mesoscale grid level. The wind speeds are subsequently modified by many atmospheric processes, and the wake evolves and is advected by the general flow, which may include realistic curvature. Hence, the wakes do not propagate in

Table 3: Annual energy production in TWh for the different wind farm blocks and the different cases. The (H) and (L) denote the highest and lowest values per case. The (*) denotes wind farm blocks that exhibit a reduced or same value when going from the non-optimized wind farm cluster to the optimized wind farm cluster layouts.

Block	Case 0	Case 1	Case 2	Case 1z	Case 2z
1	6.403	5.076	5.219	5.106	5.242
2	6.319	5.020	5.038	5.045	5.018 (*)
3	6.329	4.998	4.997	5.049	5.022 (*)
4	5.927	4.752	4.796	4.810	4.739 (*)
5	6.035	4.737	4.767	4.851	4.862
6	6.096	4.602	4.641	4.655	4.693
7	5.581	4.501	4.499	4.546	4.539 (*)
8	5.541	4.688	4.730	4.724	4.746
9	5.202	4.241	4.283	4.281	4.292
10	5.054	4.184 (L)	4.226 (L)	4.232 (L)	4.258 (L)
11	9.254	6.879	6.899	6.897	6.896 (*)
12	11.057	7.833	7.911	7.948	7.899 (*)
13	12.514	9.216 (H)	9.409 (H)	9.237 (H)	9.426 (H)
14	11.44	8.259	8.381	8.354	8.384
Cluster	102.752	78.988	79.796	79.736	80.017

unrealistic straight lines. Making the comparison of the estimates is reasonable though, because it can help in understanding the impact of each model approach's strengths and weakness.

Also of interest is the change of AEP going from non-optimized to optimized, and when increasing the area used. First for Case 1 going to Case 2, non-optimized to optimized layouts, an increase in production of 1.2 % (similar to 1.0 % determined by the mesoscale modelling) is seen. For Case 1z to Case 2z, using the larger area, going from non-optimized to optimized layouts, an increase in production of 0.3 % (simlar to 0.3 % determined by the mesoscale modelling) is seen.

Next, comparing increasing the used area, for the non-optimized cases, an increase of 0.2 %, i.e. for Case 1 to Case 1z (quite different to 0.95 % determined by the mesoscale modelling) is seen.

For the optimized cases (Case 2 to Case 2z), an increase of 0.3 % (simliar to 0.28 % determined by the mesoscale modelling) is seen.

Table 4: Wake losses for the different wind farm blocks and the different cases. The (H) and (L) denote the highest and lowest values per case. The (*) denotes wind farm blocks that exhibit a increased or same value when going from the non-optimized wind farm cluster to the optimized wind farm cluster layouts.

Block	Case 1	Case 2	Case 1z	Case 2z
1	0.207	0.185	0.203	0.181
2	0.206	0.203	0.202	0.206 (*)
3	0.210	0.210	0.202	0.207 (*)
4	0.198	0.191	0.188	0.200 (*)
5	0.215	0.210	0.196	0.194
6	0.245	0.239	0.236	0.230
7	0.193	0.194	0.185	0.187 (*)
8	0.154 (L)	0.146 (L)	0.147 (L)	0.144 (L)
9	0.185	0.177	0.177	0.175
10	0.172	0.164	0.163	0.158
11	0.257	0.255	0.255	0.255 (*)
12	0.292 (H)	0.284 (H)	0.281 (H)	0.286 (H)(*)
13	0.264	0.248	0.262	0.247
14	0.278	0.267	0.270	0.267
Cluster	0.231	0.223	0.224	0.221

Table 5: Capacity factors for the different wind farm blocks and the different cases. The (H) and (L) denote the highest and lowest values per case. The (*) denotes wind farm blocks that exhibit a reduced or same value when going from the non-optimized wind farm cluster to the optimized wind farm cluster layouts.

Block	Case 1	Case 2	Case 1z	Case 2z
1	0.560	0.576 (H)	0.563	0.578 (H)
2	0.562 (H)	0.564	0.565 (H)	0.562 (*)
3	0.543	0.543	0.549	0.546 (*)
4	0.524	0.529	0.531	0.523 (*)
5	0.522	0.526	0.535	0.536
6	0.515	0.519	0.521	0.525
7	0.496	0.496	0.501	0.501 (*)
8	0.517	0.522	0.521	0.523
9	0.475	0.479	0.479	0.480
10	0.468 (L)	0.473 (L)	0.474 (L)	0.477
11	0.476	0.477	0.477	0.477 (*)
12	0.469	0.474	0.476	0.473 (L)(*)
13	0.497	0.508	0.499	0.509
14	0.484	0.491	0.489	0.491
Cluster	0.503	0.508	0.508	0.510

Table 6: Annual energy production in TWh calculated from PyWake using the layouts in this study. See Sect. 3.1.2 for details on the calculation.

	Case 1	Case 2	Case 1z	Case 2z
Cluster	88.0651	89.0913	88.2513	89.3648

6 Conclusion and furtherwork

Four different wind turbine layout cases for the Tamil Nadu wind farm cluster have been tested for their performance characteristics using mesoscale model simulations, including EWP wind farm wake parameterization, for the representative year 2020. A reference simulation for 2020 with no wind turbine wake effects is also performed to provide wind climate statistics.

The different wind turbine layouts use uniform non-optimized layouts or optimized layouts, and exclude a 500 m internal edge zone or include that edge zone as part of the wind farm. The wind turbine layouts are optimized by Topfarm and PyWake to maximize total Annual Energy Production for the whole wind farm cluster. The optimized wind farm layouts have the same total capacity per farm as the non-optimized wind farms. The installed capacity density averaged over the wind farm areas is 5 MW/km**2.

The individual wind farm production depends on location with respect to the best wind climate and location with respect to the wake effects depending on proximity and direction of neighbouring wind farms blocks and the size of the wind farm. The wind farm performances are determined in terms of Annual Energy Production, wake losses, and Capacity Factor.

For the wind farm cluster excluding a 500 m edge zone and non-optimized layout the Annual Energy production totals 78.988 TWh. Going to the optimized layout increases the production by 1.0 % to 79.796 TWh.

For the wind farm cluster including a 500 m edge zone and non-optimized layout the Annual Energy production totals 79.736 TWh. Going to the optimized layout increases the production by 0.35 % to 80.017 TWh.

The gains can be understood in terms of ; for a wind farm with lower capacity density the potential to gain from layout optimization is smaller. Or conversely, for a wind farm with higher installed capacity density the potential to gain from layout optimization is greater. This continues until there is constraint related to turbine minimum distances between turbines that limit options for optimization.

Another interesting result is when including a 500 m edge zone for each wind farm, the wind farm cluster optimization leads to some individual wind farms having a poorer performance compared to the non-optimized layout. This was not seen when excluding a 500 m edge zone for each wind farm. This may be due to the reduced proximity of the wind farms, when there is the additional 1000 m (2 * 500 m) distance imposed between wind farms.

Increasing wind farm area gave a bigger effect for the non-optimized wind farm layouts with an increase in 0.95 %, compared to 0.28 % for the the optimized wind farm layouts. This is consistent with the thinking that when wind farm area reduces, wake losses can be mitigated to a larger extent by optimization. Again this continues until there is a constraint related to turbine minimum distances between turbines that limit options for optimization.

Further work ought to include completion of Case 1b and Case 2b which evaluates the non-optimized and optimized wind farm layouts with a new EWP wind farm parameterization, that incorporates a "layout awareness" based on PyWake modelling". This may help determine the difference between the mesoscale AEP results and the PyWake AEP results. Further understanding of the differences in these estimates is needed. It might be due to PyWake underestimating some losses due to missing mesoscale effects, including blockage. Or it might be due to the mesoscale modelling overestimating wake losses due poorer resolution of the precise placement of turbines.

Another relevant study would be to test the impact of optimizing wind farm for their own individual annual energy production. To what extent does individual optimization "harm" the overall performance of the complete wind farm cluster. Such a study can be set-up by extending the methods already outlined here.

Overall, this study has been able to supply a detailed appraisal of wind farm cluster constituent farms' performance using the state-of-the-art modelling methodologies at mesoscale and microscale. It offers insights into consequences of decisions related to using buffer zone between wind farms, and using optimizaton

of wind farm layouts. From the point of view of maximizing annual energy production, so-called "buffer zones" are not beneficial. A planning authority can use the methods outlined in this report as the starting point for the development of recommendations of utilizing the available space best, from a whole wind farm cluster energy production points of view. It should be remembered that uncertainties in the modelling methodologies, need to included in order to translate these findings into policy. Also it is important to underline that annual production is only one metric out of many that should be considered in large scale wind farm cluster design. For example, there may be other reasons for planning for gaps between wind farm "blocks". There are many other considerations, beyond wind resources, that need to be given attention in the planning process. These include, but are not limited to, seabed constraints, environmental considerations, structural loads, cabling constraints, costs related to installation, operation, maintenance, and decommissioning, levelized cost of energy considerations, market considerations (for example: the value of the electricity produced at the time it is produced) and the attractiveness to developers of the wind farm "block".

References

[1] N. O. Jensen, "A note on wind generator interaction," 1983.

[2] I. Katic, J. Højstrup, and N. Jensen, "A simple model for cluster efficiency," 1987, pp. 407–410.

[3] M. P. van der Laan, O. García-Santiago, M. Kelly, A. Meyer Forsting, C. Dubreuil-Boisclair, K. Sponheim Seim, M. Imberger, A. Peña, N. N. Sørensen, and P.-E. Réthoré, "A new rans-based wind farm parameterization and inflow model for wind farm cluster modeling," Wind Energy Science, vol. 8, no. 5, pp. 819–848, 2023.

[4] T. U. of Denmark and M.-P. I. for Biogeochemistry, "Making the most of offshore wind: Re-evaluating the potential of offshore wind in the german north sea," 2020.

[5] M. P. van der Laan, O. García-Santiago, N. N. Sørensen, N. Troldborg, J. Criado Risco, and J. Badger, "Simulating wake losses of the danish energy island wind farm cluster," in Journal of Physics: Conference Series, vol. 2505, no. 1. IOP Publishing, 2023, p. 012015.

[6] W. C. Skamarock, J. B. Klemp, J. Dudhia, D. O. Gill, Z. Liu, J. Berner, W. Wang, J. G. Powers, M. G. Duda, D. M. Barker, and X.-Y. Huang, "A description of the advanced research WRF version 4," NCAR Tech. Note NCAR/TN-556+STR, Tech. Rep., 2019. [Online]. Available: https://opensky.ucar.edu/islandora/object/opensky:2898

[7] P. J. Volker, J. Badger, A. N. Hahmann, and S. Ott, "The explicit wake parametrisation V1.0: A wind farm parametrisation in the mesoscale model WRF," Geosci Model Dev., vol. 8, no. 11, pp. 3715–3731, 2015.

[8] TOPFARM documentation. [Online]. Available: https://topfarm.pages.windenergy.dtu.dk/TopFarm2/

[9] PyWake documentation. [Online]. Available: https://topfarm.pages.windenergy.dtu.dk/PyWake/

[10] E. Gaertner, J. Rinker, L. Sethuraman, F. Zahle, B. Anderson, G. Barter, N. Abbas, F. Meng, P. Bortolotti, W. Skrzypinski et al., "Definition of the iea 15-megawatt offshore reference wind turbine," 2020.

[11] J. Quick, P.-E. Rethore, M. Mølgaard Pedersen, R. V. Rodrigues, and M. Friis-Møller, "Stochastic gradient descent for wind farm optimization," Wind Energy Science, vol. 8, no. 8, pp. 1235–1250, 2023.

[12] N. Nygaard, L. Poulsen, E. Svensson, and J. G. Pedersen, "Large-scale benchmarking of wake models for offshore wind farms," in Journal of Physics: Conference Series, vol. 2265, no. 2. IOP Publishing, 2022, p. 022008.

[13] J. G. Pedersen, E. Svensson, L. Poulsen, and N. G. Nygaard, "Turbulence optimized park model with gaussian wake profile," in Journal of Physics: Conference Series, vol. 2265, no. 2. IOP Publishing, 2022, p. 022063.

[14] A. N. Hahmann, T. S̄ile, B. Witha, N. N. Davis, M. Dörenkämper, Y. Ezber, E. García-Bustamante, J. F. González-Rouco, J. Navarro, B. T. Olsen, and S. Söderberg, "The making of the New European Wind Atlas – Part 1: Model sensitivity," Geosci Model Dev., vol. 13, no. 10, pp. 5053–5078, Oct. 2020.

[15] H. Hersbach et al., "The era5 global reanalysis," Quarterly Journal of the Royal Meteorological Society, vol. 146, no. 730, p. 1999, 2020.

[16] C. J. Donlon, M. Martin, J. Stark, J. Roberts-Jones, E. Fiedler, and W. Wimmer, "The operational sea surface temperature and sea ice analysis (OSTIA) system," Remote Sensing of Environment, vol. 116, pp. 140–158, 2012.

[17] A. N. Hahmann, R. R. Floors, C. Lennard, D. Cavar, B. T. Olsen, N. N. Davis, N. G. Mortensen, and J. C. Hansen, "Mesoscale and microscale downscaling for the wind atlas of south africa (wasa) project: Phase 3," 2021.

[18] A. C. Fitch, J. B. Olson, J. K. Lundquist, J. Dudhia, A. K. Gupta, J. Michalakes, and I. Barstad, "Local and Mesoscale Impacts of Wind Farms as Parameterized in a Mesoscale NWP Model," Mon. Wea. Rev., vol. 140, no. 9, pp. 3017–3038, Sep. 2012.

DTU Wind Energy
Department of Wind Energy
Technical University of Denmark

Risø Campus Building 118
Frederiksborgvej 399
DK-4000 Roskilde
www.vindenergi.dtu.dk

DTU Wind Energy E-0257